Welding in the World (2025) 69:2335–2350
https://doi.org/10.1007/s40194-025-02033-2

RESEARCH PAPER

Round-robin study on the determination of weld geometry parameters—part B: analysis of welded specimen

Finn Renken[1] · Jan Schubnell[2] · Matthias Jung[2] · Moritz Braun[1,3] · Heikki Remes[4]

Received: 26 September 2024 / Accepted: 28 March 2025 / Published online: 15 April 2025

Abstract
The local geometry of the weld toe or the weld seam has a high influence on the fatigue strength of welded joints. Two main parameters for the geometrical description of the weld toe are the weld toe radius and the weld toe angle. Currently, there is no uniform definition or standardized measurement approach for the assessment of these parameters. For this reason, the presented extensive round-robin (RR) study focusses on the influence of different evaluation techniques and measurement systems regarding the mentioned parameters based on 3D surface scans. In total, 20 participants take part in this two stage RR (19 participants in the second part). In this work, the results of the second part (part B) of the RR, namely the evaluation of weld toe radius and weld toe angle on real welded joints, are presented, where the actual weld toe geometry is not known a priori. For this, 22 data sets were evaluated. The data sets consist of measured values for the radius and angle of the weld toe in relation to the position along the weld seam. In general, significant variations are determined for the evaluated weld geometry parameters, especially for the weld toe radius. It is also shown that the condition of the weld toe transition has a high influence on the parameter. Particularly for weld seams with a low weld toe angle, the measurement results for the radius of the individual participants show high variations. For small weld toe radii, the results are quite comparable between the participants. The results for the weld toe angle are comparable for flat welds, but a wide range of results is observed for sharp weld toes. The degree of automation of the measurement method also has a high influence on the results. The most accurate results are expected from manual measurements, while the fully automatic and semi-automatic methods show larger deviations.

Keywords Weld toe measurement · Weld toe radius · Weld toe angle · Local weld toe geometry · Weld scans

1 Introduction

Weld geometry parameters play an important role in determining the structural integrity, mechanical performance, and, in general, the quality of welded joints as outlined by several standards [1–3]. Precise characterization is essential to ensure the quality and fatigue strength of welds in various applications, ranging from aerospace and automotive to construction and shipbuilding industries. As welding processes continue to evolve, the demand for advanced automated methodologies to accurately describe weld geometry parameters has become increasingly important.

Recommended for publication by Commission XIII—Fatigue of Welded Components and Structures

✉ Jan Schubnell
jan.schubnell@iwm.fraunhofer.de

Finn Renken
finn.renken@tuhh.de

Matthias Jung
matthias.jung@iwm.fraunhofer.de

Moritz Braun
moritz.braun@dlr.d

Heikki Remes
heikki.remes@aalto.fi

[1] Institute for Ship Structural Design and Analysis, Hamburg University of Technology, Hamburg, Germany

[2] Fraunhofer Institute for Mechanics of Materials IWM, Freiburg, Germany

[3] German Aerospace Center (DLR), Institute of Maritime Energy Systems, Geesthacht, Germany

[4] Aalto University, Espoo, Finland

Important weld geometry parameters, as shown in Fig. 1, describing the overall weld shape include weld width, penetration depth, reinforcement height, and heat-affected zone dimensions. In addition, fatigue strength is significantly affected by the local notch shape at weld transitions, which include weld toe radii, notch opening, and weld toe angles, and undercut depth [3–9]. The correlation between these parameters and the fatigue strength of welded joints is well-known [4, 5, 10]. The local geometrical parameters, like weld toe radius, are influenced by a variety of factors such as welding technique and position, heat input, welding speed, and the properties of the base and filler materials [11]. Understanding the interaction between these factors and their impact on weld geometry is crucial for optimizing welding processes and achieving desired mechanical properties in the weldment.

Traditional methods for measuring weld geometry parameters often involve destructive testing and manual inspection, which can be time-consuming, labor-intensive, and subject to human error. In contrast, advanced non-destructive testing (NDT) techniques, computational modeling, and automated inspection systems offer significant advantages in terms of accuracy, efficiency, and repeatability. These modern approaches enable a more comprehensive analysis of weld geometry and provide valuable insights into the results of welding process parameters; however, the development of such automated inspection systems is complex and time-consuming as well. For example, the determination of a suitable sampling rate, i.e., the frequency of measurements, is cumbersome; see [12, 13]. There are both commercial and research systems available for weld geometry assessment that can be divided into manual (where the area of interest (AOI) for fitting of the geometrical parameter is selected manually), semi-automatic (where the AOI is defined manually, but fitting is performed automatically), and fully automatic (where the AOI and fitting is performed automatically) measurement systems. The development of automatic and semi-automatic systems relies on several assumptions to, e.g., find the weld transition area (AOI); however, even the development of a digital measurement system, which is operated manually, has its challenges [14].

The present round-robin study was initiated to compare different approaches to measuring and describing the geometry of welded joints and develop a general understanding of the accuracy with which geometrical parameter of welded joints can be determined based on 3D scans. The primary objectives of this study are to test and compare different methods for the determination of weld geometry parameters using state-of-the-art techniques. For this, two stages of the round-robin study were organized. In the first part (part A), a machined specimen with known geometry resembling a cruciform joint was analyzed, and the results were compared with the actual dimensions of the specimen [15]. This work presents the results of the second part (part B) based on real welded specimens. Several small-scale specimens representing weld geometries of various types were selected and circulated between the 20 participants of the round-robin study. Subsequently, the results of the participants are presented and compared using information about the measurement techniques.

This study seeks to advance the field of welding engineering by providing detailed insights into weld geometry characterization. The outcomes are expected to contribute to the development of improved welding characterization practices, weld quality standards, and more reliable structural integrity assessments of welded joints.

2 Overview

Of the 19 participants, some use multiple evaluation methods or digitizers, resulting in a total of 22 data sets. No specific recommendations regarding evaluation algorithms, measurement systems, specimen preparation, or even the definition of weld toe radius and weld toe angle were provided prior to the study. All evaluation methods, however, rely on 2D section cuts along the weld seam. Weld toe radii and weld toe angles are determined with respect to a z-coordinate running along the weld seam.

Six different digitizer types are employed, as summarized in Table 1.Most participants use either fringe projection (FP) or laser line (LL) sensors. Light sectioning methods, such as FP or LL, work based on the triangulation of a projected light pattern that is deformed by the surface topology, as illustrated in Fig. 2a. Chromatic confocal sensors, by contrast, employ a white light spectrum in which specific colors

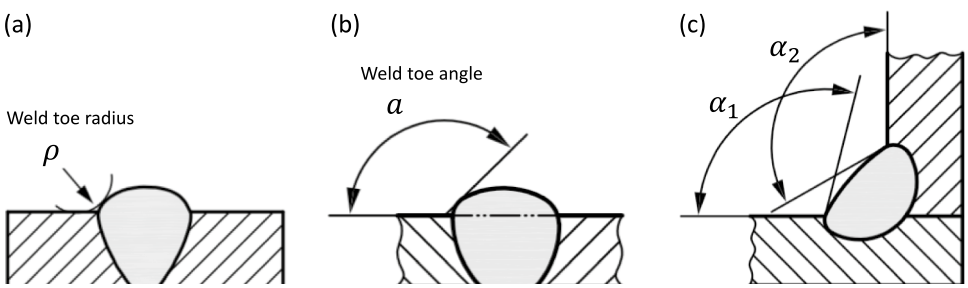

Fig. 1 Illustration of weld toe radius ρ and weld toe angle α according to ISO 5817 [1]

Table 1 Digitizers and abbreviation

Digitizer	Abbreviation	Number of data sets
Fringe Projection Sensor	FP	8
Laser Distance Sensor	LD	1
Laser Line Sensor	LL	9
Line Confocal Imaging	LC	1
Microscopy	MI	2
Roughness	RO	1

Table 2 Automation and abbreviation

Automation	Abbreviation	Number of data-sets
Automated	A	5
Semi-Automated	SA	10
Manual	M	7

Table 3 Participant overview

Data Sets	Resolution in plane [µm]	Resolution out of plane [µm]
P01	8.1	0.98
P02	10	10
P03	1	1
P04	12.5	20
P05	39.1	4
P06	0.1	0.1
P07	10	0.5
P08	-	-
P09	0.1	0.1
P10	2.25	20
P11	2.25	20
P12	63	63
P13	50	50
P14	0.5	0.4
P15	13	10
P16	70	10
P17	80	13
P18	5	0.1
P19	300	-
P20	25	25
P21	25	25
P22	60	2

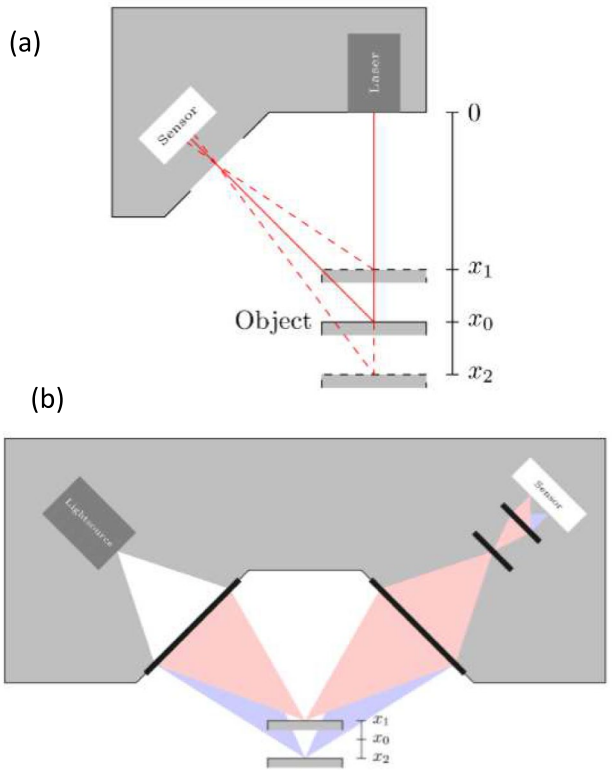

Fig. 2 **a** Point projection, **b** chromatic confocal surface profiling

correspond to known distances from the sensor. A peak in the reflected spectrum's intensity indicates the distance to the surface, as depicted in Fig. 2b.

Participants assign themselves to one of three predefined automation grades, as shown in Table 2: fully automated, semi-automated, and manual. These automation grades are defined as follows: Fully automated evaluations involve the detection of the area of interest (AOI) and the fitting procedure for the geometrical parameters to be carried out without user intervention. Semi-automated evaluations require some manual input, such as selecting t2he AOI or defining the measuring range, while other steps are automated. Manual evaluations necessitate that all steps be performed by the user. Most participants classify their evaluations as semi-automated.

Regarding data filtering and specific algorithms, this information is not standardized or collected. Participants determine their own processes, including whether to apply filtering to their measurements or not. Since this information is not reported, the impact of filtering or specific algorithmic choices cannot be assessed.

Due to the large number of different digitizers, the individual digitizers also have different resolutions. An overview of all participants with their respective digitizers, automation, and resolution is shown in Table 3.

It was not specified how many sections should be measured. This results in quite different numbers of data points

(see Table 4). The automated and semi-automated methods usually measured significantly more slices, while the manual methods only measured at very few points on the weld seam, as the measurement effort here is many times higher. In addition, some participants did not report data for all weld toes (WT).

3 Specimens

Three different specimens are used and are scanned by each participant. The samples are labeled IIW-A, IIW-B, and IIW-C. Four weld toes of each specimen are used for the evaluation. The specimens are shown in Fig. 3. For the fillet welds (see IIW-A and IIW-B), only the weld toes that represented the transition from the base plate to the welded joint are evaluated. All samples have a pre-defined coordinate system for each weld toe, shown in Fig. 3. The z-coordinate is defined along the weld seam. All measurement results are assigned to a z-coordinate along the weld seam. This allows for the comparison of the measurement results according to their position. The cross sections of all investigated welds are given in Fig. 4. The roughness of the specimens ranges between Rz of 19 and 25 µm in accordance with ISO 4287–1:1997.

3.1 Specimen IIW-A

Specimen IIW-A is a transverse stiffener made of structural steel S355 J2 + N by gas metal arc welding (GMAW) with a plate thickness of 10 mm and a width of 130 mm, as shown in Fig. 4. Detailed information about the manufacturing process is given by Schubnell et al. [16]. The four welded joints of the specimen have different conditions: Weld 1 with weld toe (WT) 1 is a single layer fillet weld with a throat thickness of 5 mm that was welded automatically; weld toe 2 and weld toe 3 are part of manually welded repair welds with a lower toe angle; weld toe 4 is similar to weld toe 1 but was post weld treated by high-frequency mechanical impact (HFMI).

3.2 Specimen IIW-B

Specimen IIW-B is the only butt weld among the specimens. It has a V weld shape and was welded from one side with a backing bar. This creates a predefined weld seam root. The sample was made of S500G1 + M steel by flux-cored arc

Table 4 Number of slices of each weld

Data Sets	Digi- tizer	Auto- mation	Weld											
			A				B				C			
			A-W1	A-W2	A-W3	A-W4	B-W1	B-W2	B-W3	B-W4	C-W1	C-W2	C-W3	C-W4
P01	LC	SA	11	11	11	11	11	11	11	11	11	11	11	11
P02	FP	M	5	5	5	5	4	4	4	4	4	4	4	4
P03	LD	SA	3	3	3	3	3	3	3	3	3	3	3	3
P04	LL	SA	800	800	800	800	400	400	400	400	400	400	400	400
P05	LL	SA	1275	1251	1216	1264	511	495	504	509	462	490	460	416
P06	FP	M	4	4	4	4	4	4	4	4	4	4	4	4
P07	LL	M	38	38	31	31	31	31	31	31	31	31	31	26
P08	LL	SA	251	248	249	250	90	92	88	88	98	97	98	98
P09	RO	M	0	4	0	4	4	4	4	4	4	4	4	4
P10	MI	SA	16	16	16	16	8	8	8	8	8	8	8	8
P11	MI	SA	0	0	0	16	8	8	8	8	8	8	8	8
P12	LL	M	10	10	10	10	10	10	10	10	10	10	10	10
P13	LL	A	124	122	121	121	33	41	39	34	44	44	45	45
P14	FP	M	9	9	9	9	9	9	9	9	9	9	9	9
P15	LL	SA	3	3	3	3	3	3	3	3	3	3	3	3
P16	LL	A	300	300	300	300	300	300	300	300	300	300	300	300
P17	FP	A	123	123	123	123	97	97	99	99	97	97	97	97
P18	FP	A	0	0	0	0	99	99	99	99	0	0	0	0
P19	FP	M	5	5	5	5	5	5	5	5	5	5	5	5
P20	FP	SA	260	262	260	260	150	150	150	150	150	150	150	150
P21	FP	SA	260	262	260	260	150	150	150	150	150	150	150	150
P22	FP	A	128	128	128	128	51	51	51	51	51	51	51	51

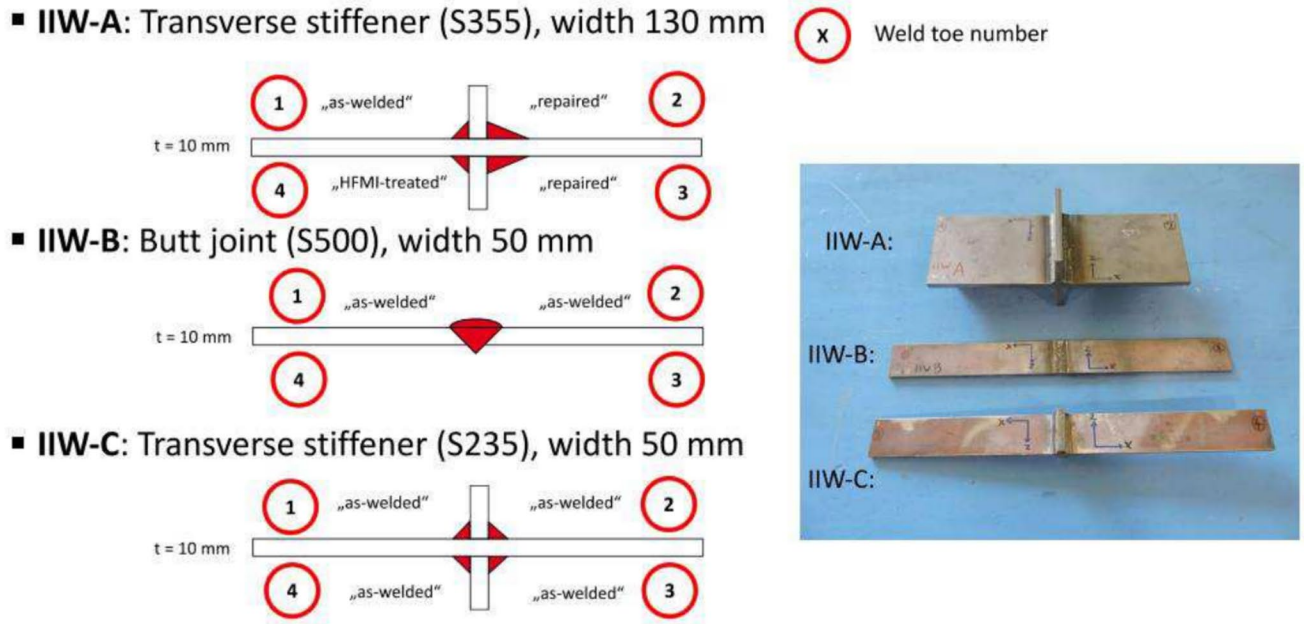

Fig. 3 The three specimens measured by each participant with specimen IIW-A at the top, specimen IIW-B in the middle and specimen IIW-C at the bottom

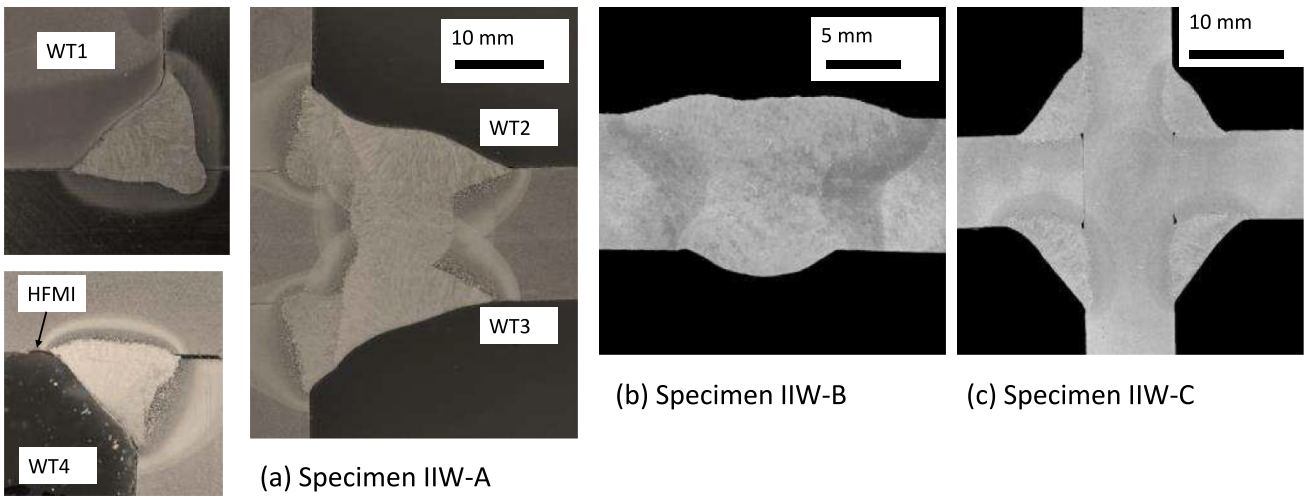

Fig. 4 Micrographs of the welded test specimens of the round-robin study

welding (FCAW) and has a thickness of 10 mm and a width of 50 mm. All 4 weld toes are in the as-welded condition, but have a high weld quality for butt joints. More information and fatigue test results for this high-quality welded joint can be found in Braun et al. [17].

3.3 Specimen IIW-C

Specimen IIW-C is another fillet-welded specimen. However, it is a load-carrying cruciform joint and smaller than specimen IIW-A. It has a width of 50 mm and is made of S235 J2 +N steel. Similar to specimen IIW-B, it was made by the FCAW process. Like the other samples, it has a thickness of 10 mm. All four weld toes are in the as-welded condition. More information can be found in Braun et al. [18].

4 Results

Box plots and line plots are used to display the weld toe radii and weld toe angles for all weld toes. The box of the box plots shows the interquartile range (IQR), which spans from the first quartile (Q1) to the third quartile (Q3), encompassing the middle 50% of the data. In the box, the median is marked as a red line. Q1 - 1.5·IQR defines the lower whiskers and Q3 + 1.5·IQR defines the upper whiskers. Points outside the whiskers are declared as outliers and are marked with an *x*.

The results are summarized in groups to determine the influence of the participants, measurement systems (digitizers), and automation. The data are not subsequently filtered. This can lead to significant outliers in some cases, which are not shown in every figure. For a clearer representation, the *y* axes are limited. For box plots, the range between 0 and 20 mm is shown for the radius and between 100 and 200°.

The actual weld toe geometry parameters are unknown. For this reason, a global median is formed in the box plots from all median values of the individual data sets for the purpose of comparability. This forms an approximation across all data sets, which makes it possible to make a statement about the scattering of the individual data sets.

For better comparability of the line plots, a minimum number of data points are used, as the number of points of the individual participants along the seam varies significantly (see Table 4). Therefore, 200 data points are used for each line plot. This means that the points are either reduced or interpolated. This increases comparability, as measured or interpolated values at the same position can be compared. The measurement range is adapted to the sample width. The results are sorted by the weld geometry, the automation degree, and the digitizer.

4.1 Weld geometry

The results regarding weld toe radius and weld toe angle are displayed in Fig. 5 for the evaluation of fillet welds. Almost all participants show a comparable low scatter for the weld toe radius ρ of specimen IIW-A while the results of the weld toe angle α has a much higher scatter (see Fig. 5a). Half of the results (11 out of 22) meet the global median of weld toe radius $\overline{\rho}$ (which means that the global mean value of the weld toe radius $\overline{\rho}$ is inside the range of Q1 to Q3). The global mean values $\overline{\rho}$ and $\overline{\alpha}$ for both parameters are summarized in Table 5. The results of ρ of weld toe 3 of specimen IIW-C, however, show a higher scatter while the global median $\overline{\rho}$ is met again by half of the participants (see Fig. 5c). For the angle, there are also no comparable results between the participants for both specimens (see Fig. 5b and d). The global median values $\overline{\rho}$ and $\overline{\alpha}$ is not met by most of the participants.

Figure 6 shows the results for butt joint (specimen IIW-B). Different geometrical parameters were evaluated for top side and the weld root side by all participants. The results of ρ show a clear distinction between the top and the bottom of the weldment. Figure 6a shows the measurement results of weld toe 2, which is the top weld. Again, half of the participants met the $\overline{\rho}$ value. In Fig. 6c, the same results are shown for weld toe 3 (weld root side). The scatter and the measured radius are much lower for all data series compared to the values from weld toe 1. In this case, the majority of the data series (19 out of 22) met the $\overline{\rho}$ value. Such a difference in the scatter is not visible regarding the results of weld toe angle α (see Fig. 6b and d). The scatter and the distance to the global median are comparable. However, all participants show higher measured values for the upper weld toes.

The results of the geometrical parameters of the welded joints in repaired condition (specimen IIW-A, weld toe 2 and weld toe 3) are shown in Fig. 7. Note, that these welds are characterized by a flat weld toe. The weld toes are measured by 19 of the 22 participants. In contrast to weld toe 1, a significantly higher scatter of the radii ρ can be seen. This is shown in Fig. 7a using weld toe 3. For the angle, the difference from the global median is relatively small. All angle measurements are arranged along the global median.

The results for the HFMI-treated weld are displayed in Fig. 8. This leads to significantly more uniform radius measurements for all data series (see Fig. 8a). In contrast, there are significantly greater variations in the angular measurement (see Fig. 8b). Some participants have a much higher scatter compared to the others while others have a large deviation from the global median.

4.2 Automation

The results classified according to the degree of automation are plotted in Fig. 9. The participants themselves classified the automation according to the criteria mentioned in Sect. 2. Data series using the manual measurements have the lowest scatter and semi-automated measurements have the highest. However, it should be noted that some of the data series contain significantly lower numbers of measured slices (Table 2). For the angle, on the other hand, the scattering of the manual method is comparable to that of the automatic and semi-automatic methods. The scatter of the automation method is shown in Fig. 9 for weld toe 1 of specimen IIW-A. The median of each method is similar. The violin plots for the radius are truncated at zero because radius values below this threshold are physically implausible and do not occur in the measurement data.

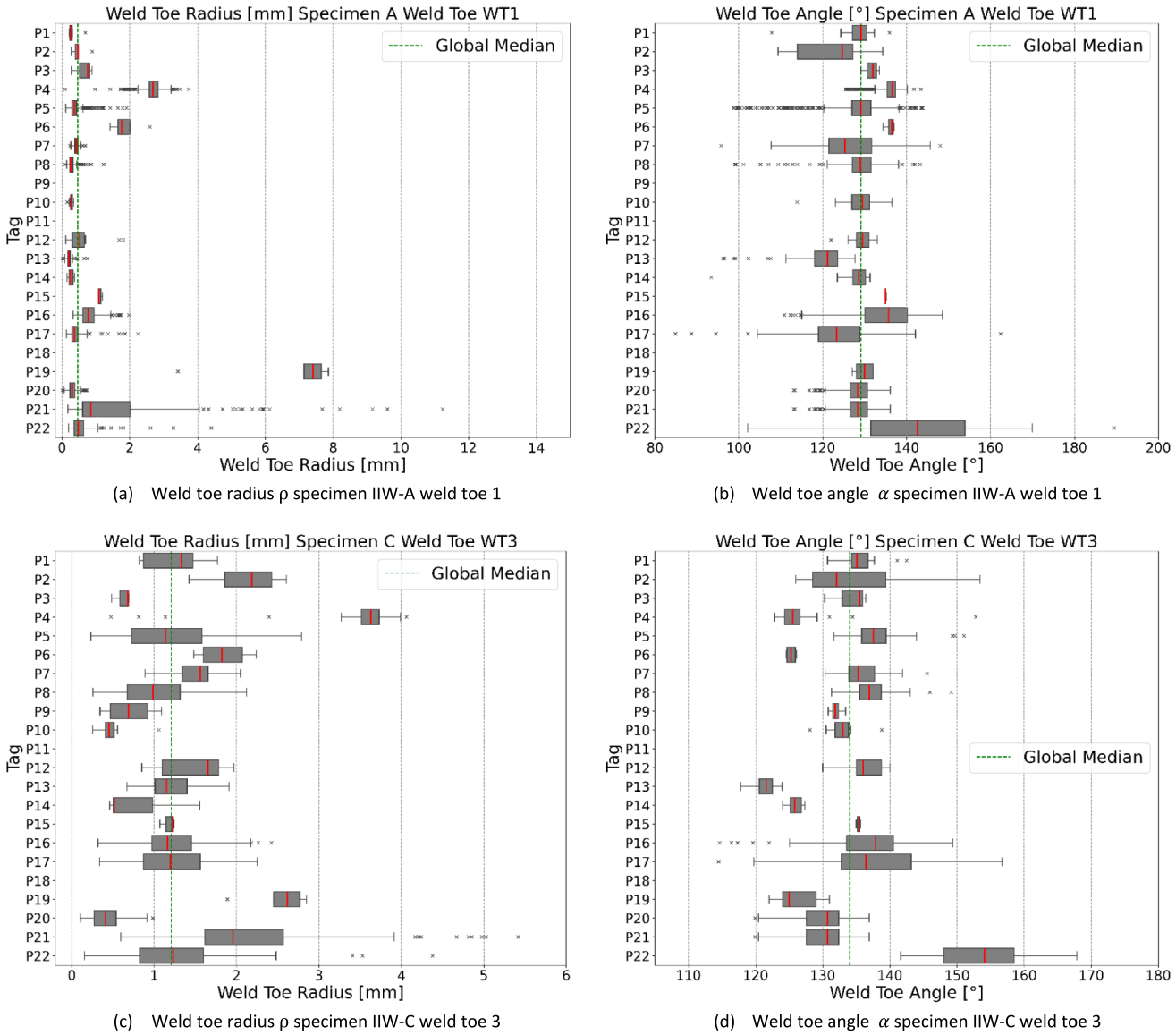

(a) Weld toe radius ρ specimen IIW-A weld toe 1

(b) Weld toe angle α specimen IIW-A weld toe 1

(c) Weld toe radius ρ specimen IIW-C weld toe 3

(d) Weld toe angle α specimen IIW-C weld toe 3

Fig. 5 Results of geometrical parameter at fillet welds

Table 5 Global median of weld toe radius $\overline{\rho}$ and weld toe angle $\overline{\alpha}$

Parameter	specimen IIW-A				specimen IIW-B				specimen IIW-C			
	A-WT1	A-WT2	A-WT3	A-WT4	B-WT1	B-WT2	B-WT3	B-WT4	C-WT1	C-WT2	C-WT3	C-WT4
$\overline{\rho}$[mm]	0.465	2.451	3.147	1.916	1.323	2.401	1.429	1.746	1.312	1.389	1.210	2.309
$\overline{\alpha}$ [°]	129.10	161.28	160.45	127.69	162.71	159.90	151.67	148.03	142.36	137.81	134.05	132.77

Figure 10 shows the results for weld toe 3 (repaired condition) and the HFMI-treated weld toe 4 (HFMI-treated) of specimen IIW-A. Here z describes the position along the weld seam. Figure 3 shows the definition of z on the samples. As all datasets have a different number of data points, this results in different curves and measurement ranges.

The variation of the results from the weld toe radius of weld toe 3 is comparably low for the automated case; see Fig. 10a. The results for the weld toe angle α are quite similar; see Fig. 10b. The uniform measurement results for the HFMI-treated weld toe can be seen for all degrees of automation; see Fig. 10c. The results plotted in Fig. 10d

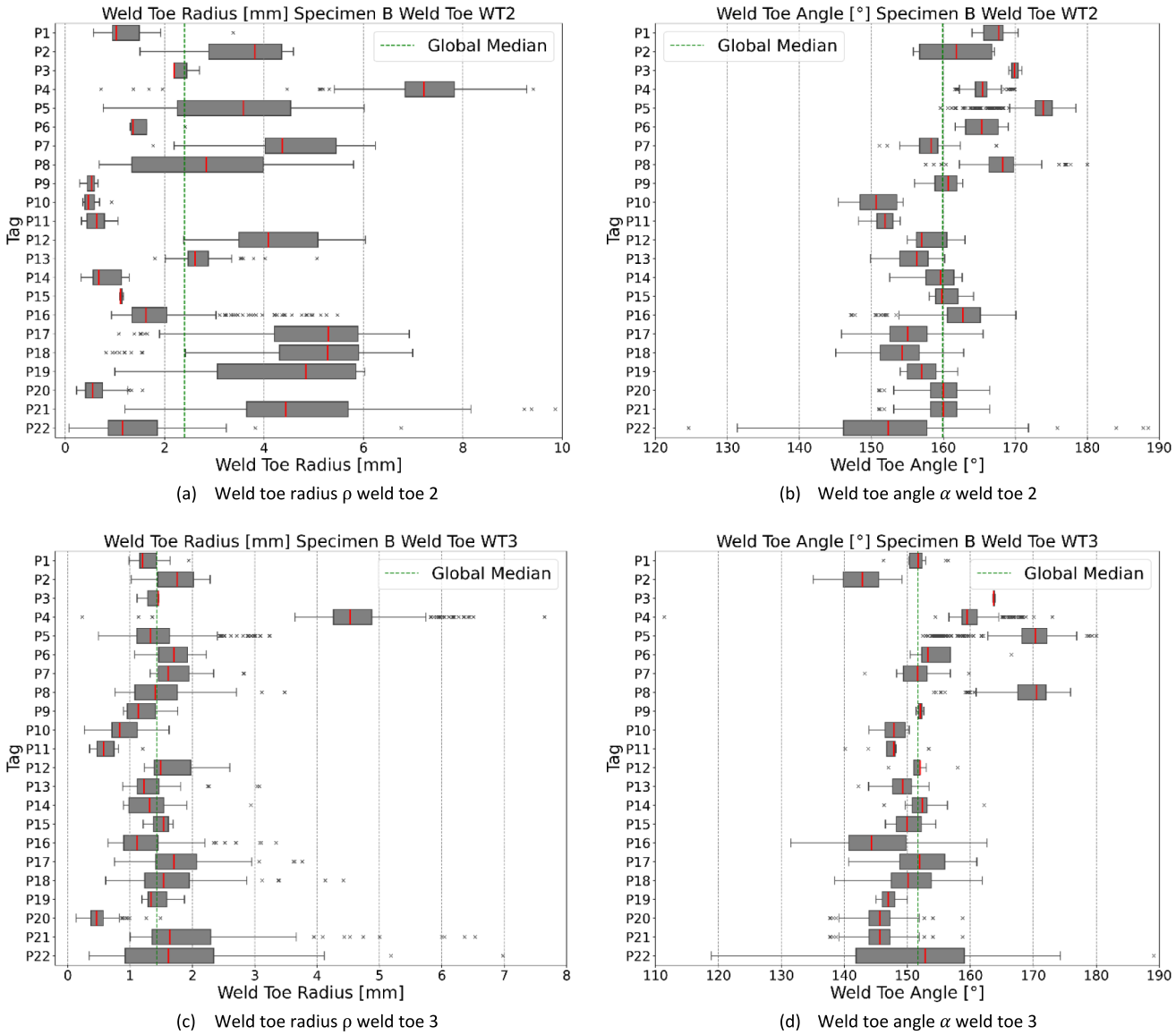

Fig. 6 Box plot of the participants for weld toe 2 and 3 of specimen IIW-B for the radius and angle

(HFMI-treated welded joint) shows that the strong scattering of the weld toe angle α measurements is mainly related to the automated methods, while the strong outliers tend to be due to the semi-automated measurements. The manual measurements show less scatter.

While the results of the repaired-welded welds (specimen IIW-A weld toe 2 and 3) show the highest variation of weld toe radius ρ, the HFMI-treated weld shows the highest regarding the weld toe angle α. Only the results of the weld toe angles evaluated by manual methods have a low scatter. To illustrate this effect, the measured values for the radius in Fig. 11 and the measured values for the angle in Fig. 12 are shown along the weld toe for data series per automation degree. For the radius of the repaired weld toe, the measured radii exhibit a high scatter and different values at the corresponding z coordinates (see Fig. 11a). For the weld toe angle measurement, only the automated methods have a high scatter in Fig. 12a. The other degrees of automation show comparable results along the weld toe. The radius of the HFMI-treated weld toe has the highest scatter of the automated method (see Fig. 11b). The semi-automated method shows small scatter along the different data sets, but the amplitudes of the weld toe radius are different. However, manual measurements have the smallest scatter. The same effect of the different degree of automation can be seen for the angle in Fig. 12b.

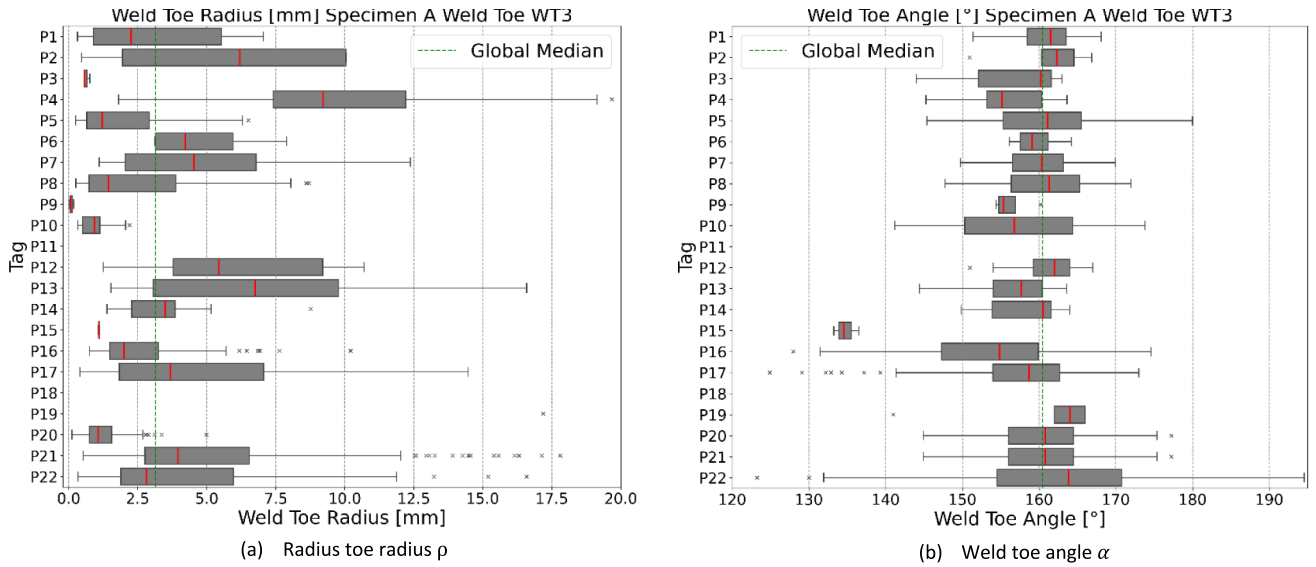

Fig. 7 Box Plot of the data series for weld toe 3 of specimen IIW-A for the radius and angle

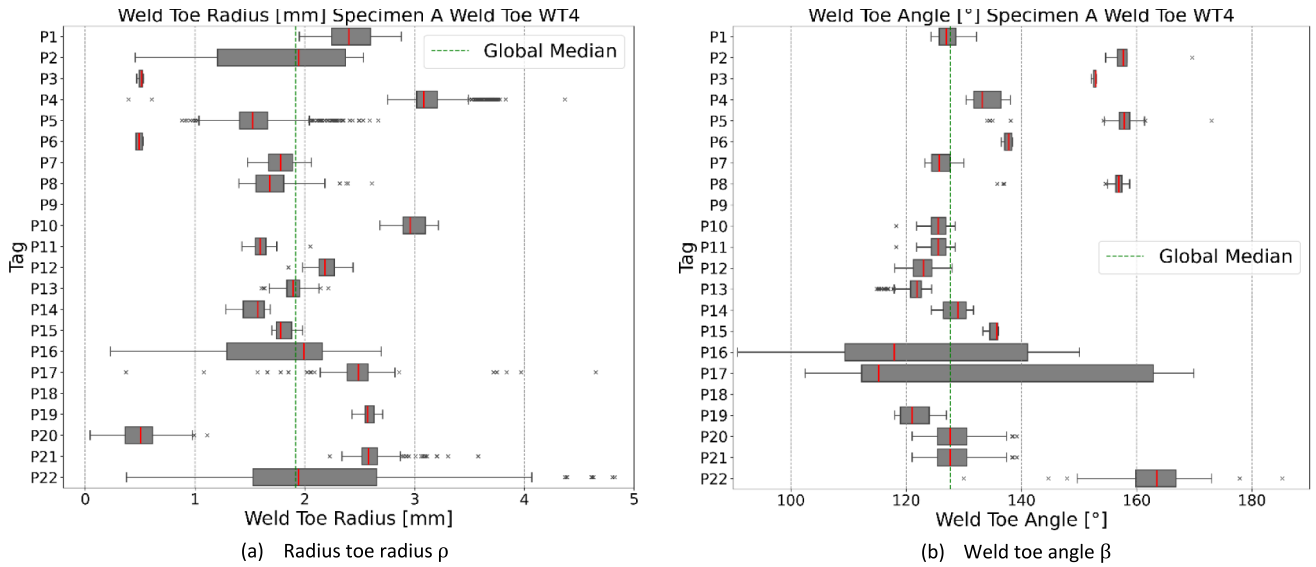

Fig. 8 Box Plot of the data series for weld toe 4 of specimen IIW-A for the radius and angle

4.3 Digitizer

The results categorized by different digitizers are plotted in Fig. 13 and are comparable for all weld toes. As most of the participants use LL and FP, the scatter is higher for these digitizers. However, the measurement results between the two are comparable. Only the scattering of the angle is usually somewhat greater with LL. This effect is shown exemplarily for specimen IIW-B in Fig. 13. The previously described difference between top and bottom weld toes can also be seen.

5 Discussion

The data of the individual data series strongly differ for most welds. The evaluation is complicated because the number of single results differs between the data series; see Table 4. The scatter of the data is thus not directly comparable in all cases.

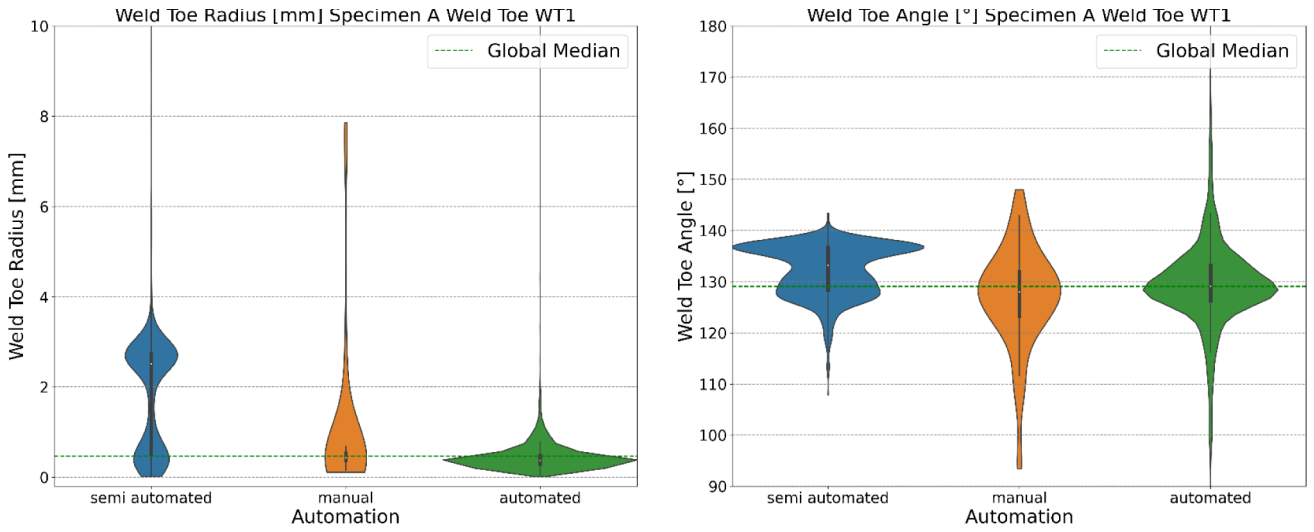

(a) weld toe radius ρ (b) Weld toe angle α

Fig. 9 Violin plot of the automation for weld toe 1 of specimen IIW-A for the radius and angle

5.1 Influence of the weld geometry

As the real parameters of the weld toes are unknown, the accuracy of the measurement results cannot be verified in the same way as in part A of this RR-study. For this reason, the accuracy of the measurement results is quantified by their deviation from the global median. It turns out that the weld seam type and state has a very high influence on the measurement results compared to the results of the part A study [15]. The weld toe 3 and weld toe 4 of specimen IIW-A, which were manually repair-welded, show very large deviations in the weld toe radius measurement; see Fig. 7a. However, the definition of the angle seems to be much more uniform among the data series. It is assumed that the flat weld makes it difficult to identify the weld toe. This results in very different measurements of the weld toe radius as well as weld toe angle.

Weld toe 4 of specimen IIW-A is used to evaluate the measured weld toe radius in detail. A uniform weld toe radius is created by the HFMI process. The line plot in Fig. 11b shows different amplitudes of the radius for the participants. However, the scatter is strongly reduced. That is not the case for the weld toe angle measurement (see Fig. 12b) and can be caused by the definition of the weld toe angle. The HFMI process significantly changes the weld toe. In principle, the angle can be measured at different positions of the weld toe. This is shown in Fig. 14. Either the plate is used as a reference or a new reference line is created in the HFMI treatment area. It is therefore possible to determine a local weld toe angleα_1 or global weld toe angle α_2. This may explain that sometimes quite large or quite small angles were measured.

Lower deviations of the results are observed in as-welded condition compared to HFMI-treated condition. However, the results of specimen IIW-B show a clear difference between the top and the weld root of a butt weld. There is a sharp weld toe at the weld root, while the weld toe on the upper side is much flatter; see Fig. 13.

5.2 Influence of the automation

The manual measurements achieve the best results compared to the global median values with a low scatter of the data. However, the manual measurements also have the lowest number of slices, which may lead to small scatter and represent the comparable high measurement effort. Single values of ρ and α along the weld seam exhibit large deviations between the measurements of different participants. The largest difference from the global median and the largest scatter for the measurement of weld toe radii and weld toe angles are usually found in the semi-automated method. Here, the automated methods usually achieve better results. As the results were not checked for plausibility, there are often incorrect measurements and therefore outliers for the automated and semi-automated methods. With a manual method, the result is checked for plausibility during measurement. This can explain the better performance of the manual method. However, due to the increased effort involved in the manual method, only a few measuring points are possible, while the automated and semi-automated can measure a large number of slices in a short time.

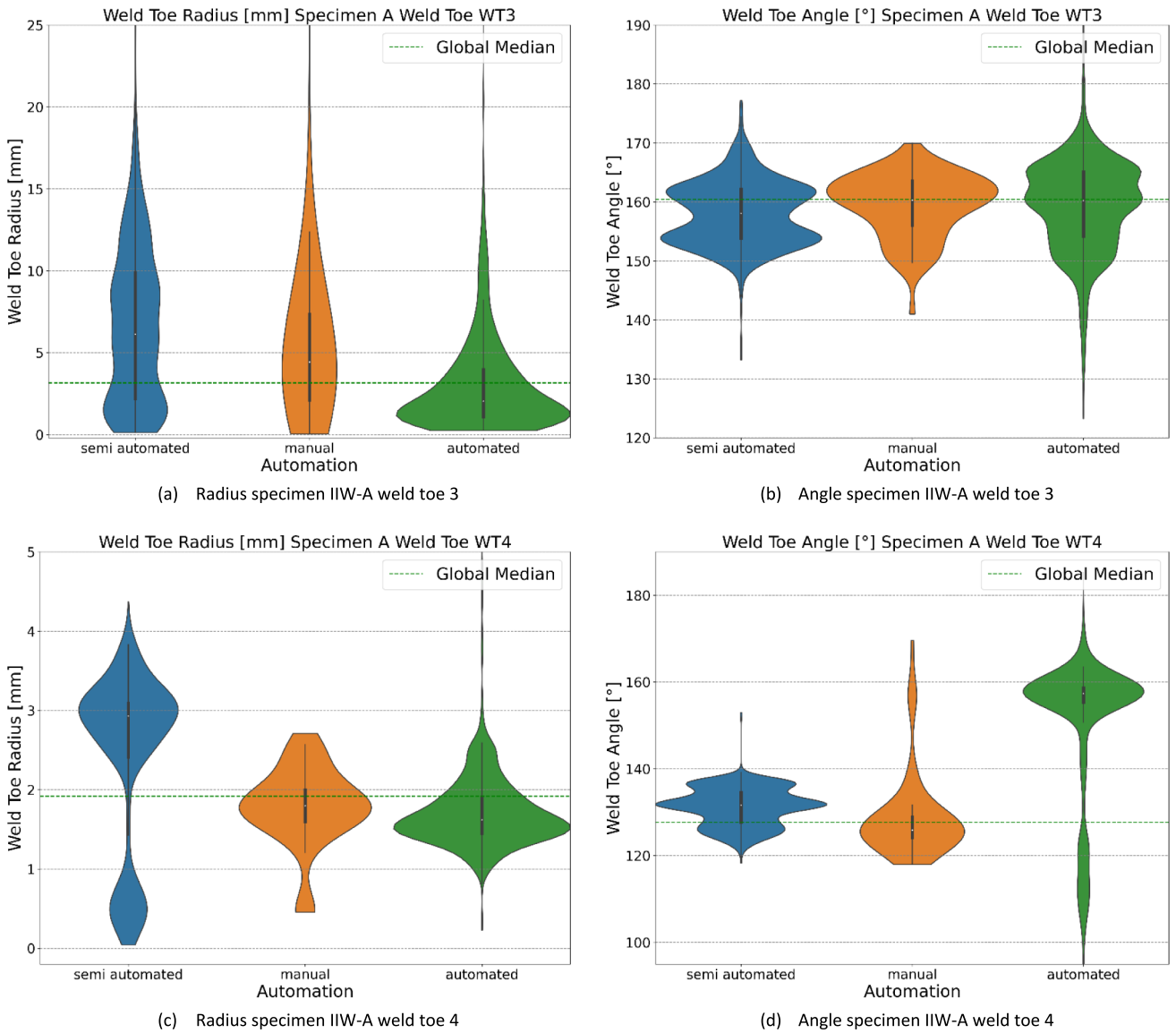

(a) Radius specimen IIW-A weld toe 3

(b) Angle specimen IIW-A weld toe 3

(c) Radius specimen IIW-A weld toe 4

(d) Angle specimen IIW-A weld toe 4

Fig. 10 Violin plot of the automation for weld toe 3 and weld toe 4 of specimen IIW-A for the radius and angle

5.3 Influence of the digitizer

Since most participants use LL and FP digitizers, a comparison is difficult (see Table 1). With only one or two participants per digitizer, a comparison is not possible because of the much higher influence of the evaluation method. For this reason, only the LL and FP digitizers can be compared with each other. Both digitizers show comparable results. This means that the influence of the digitizer is not very pronounced, but rather the following evaluation method.

5.4 Comparison to RR part A

As mentioned, in contrast to part A of this study, the real weld toe geometry is not a priori known for the specimens. Part A shows mainly comparable measurements results for a certain range of ρ and α. This is not the case in part B; see Fig. 6b and d. With flatter weld seams, on the other hand, uniform results can be seen again for weld toe angles; see Fig. 7b. However, with flat weld seams, there are large deviations in the radius measurement of the individual participants, which can be seen in Fig. 7a. In these measurements, all participants recorded large weld toe radii ($\rho > 4$ mm). While part A produced more consistent measurement results for larger radii in the machined specimen, this is not the case for the welded specimens analyzed here. The results are very scattered and there are no uniform measurement results. The scatter for the smaller radii seems to be reduced. This can be seen at specimen IIW-B in Fig. 6. The radius of the top weld toe

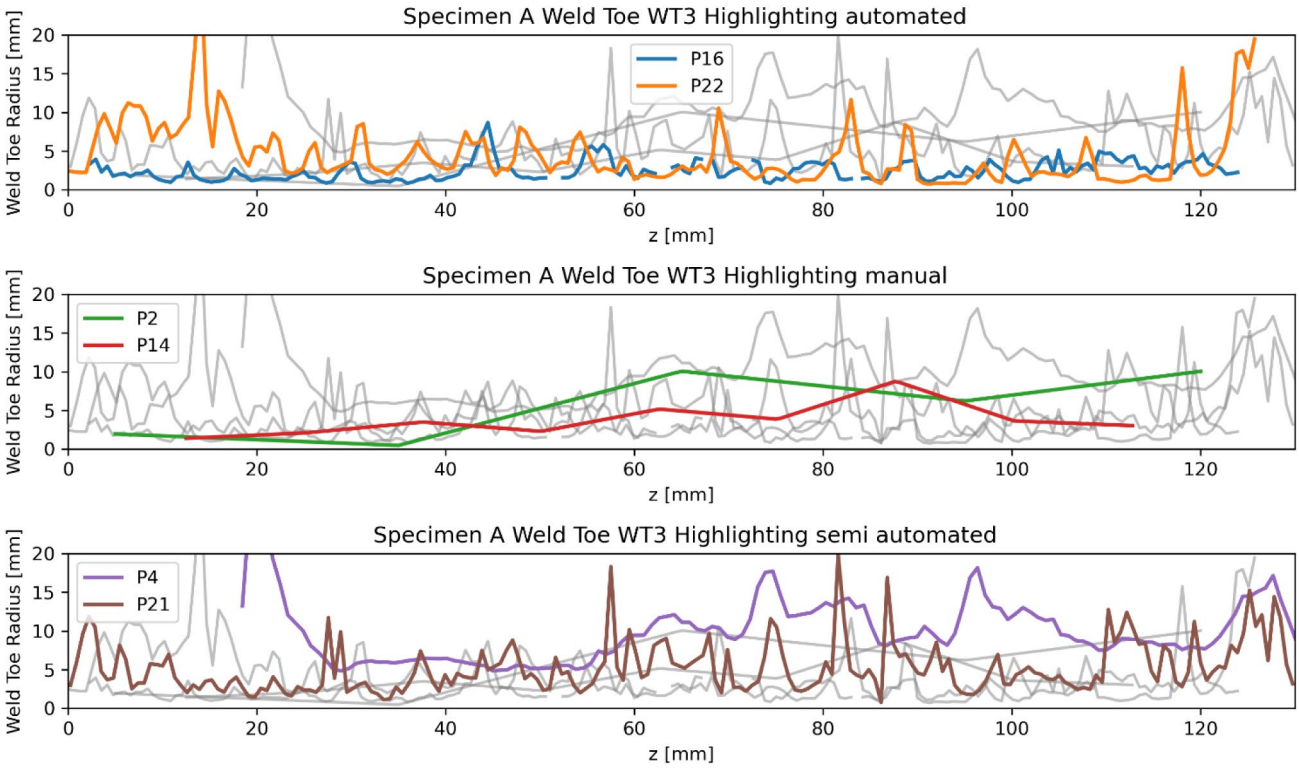

(a) Weld toe radius of weld toe 3

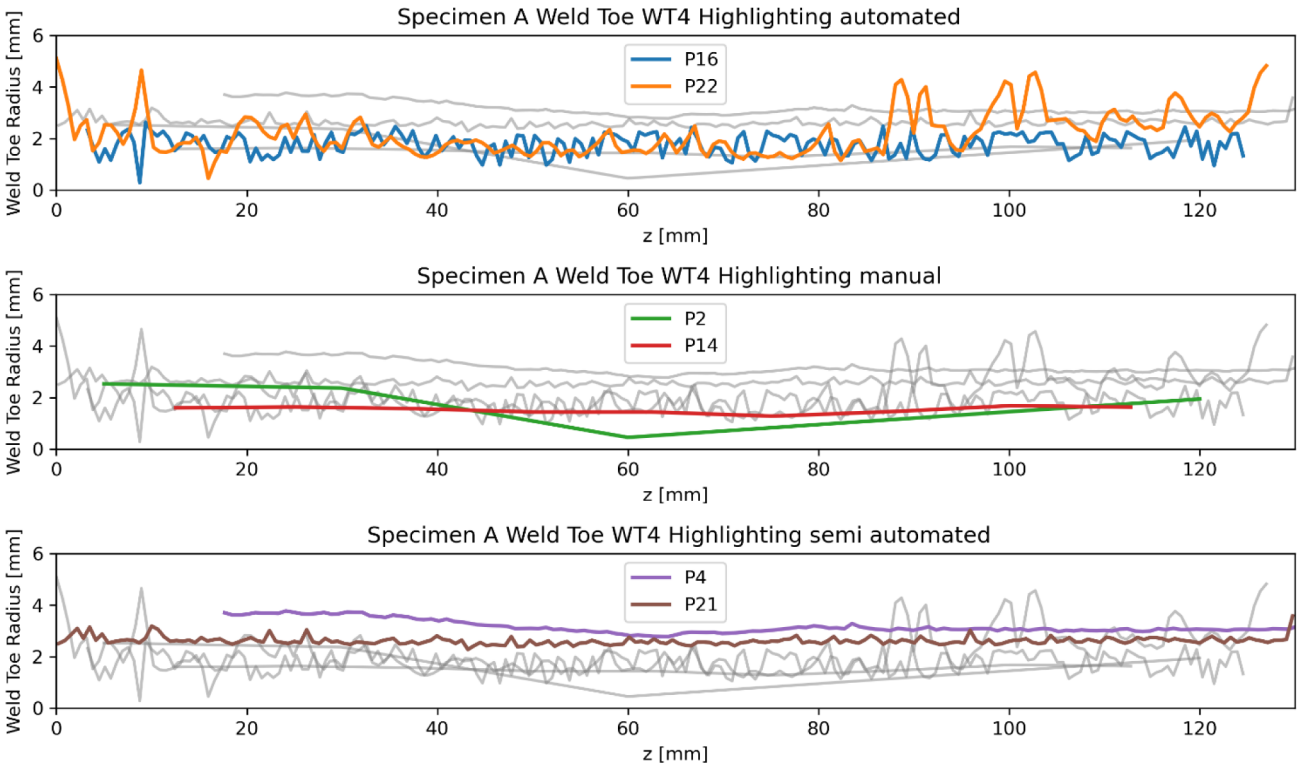

(b) Weld toe radius ρ of weld toe 4

Fig. 11 Line plot of the weld toe radius ρ for different degree of automation of specimen IIW-A

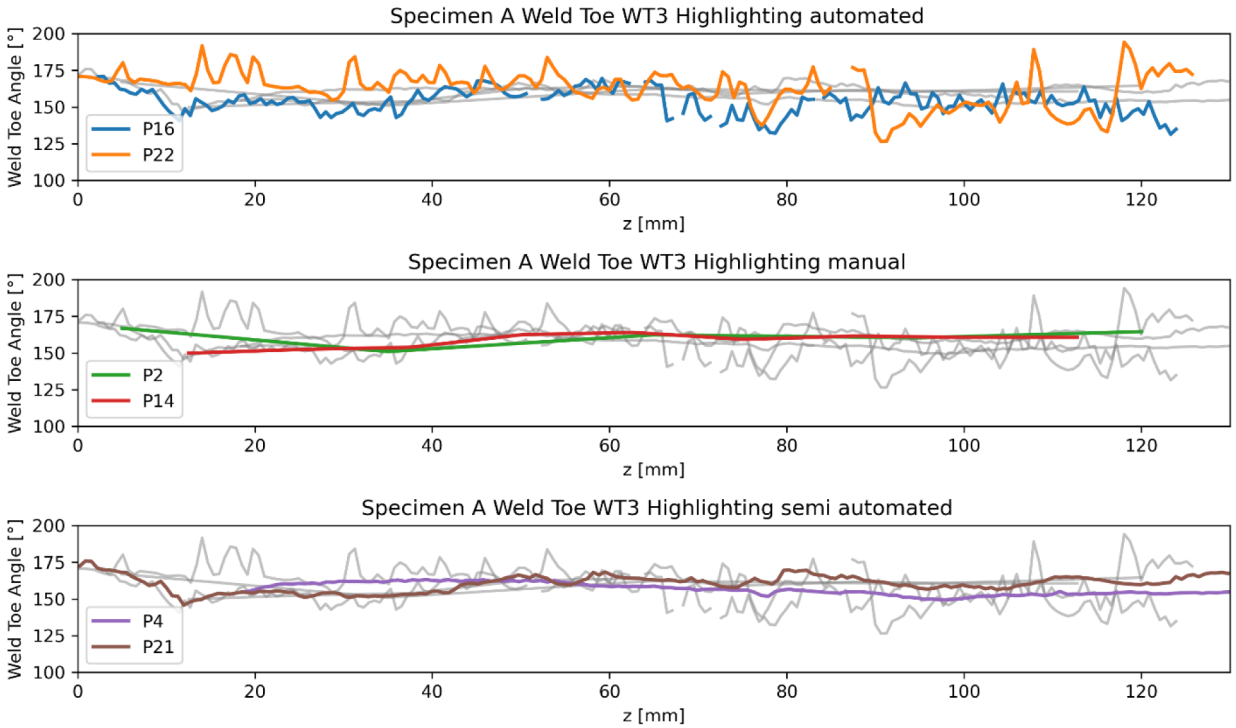

(a) Weld toe angle of weld toe 3

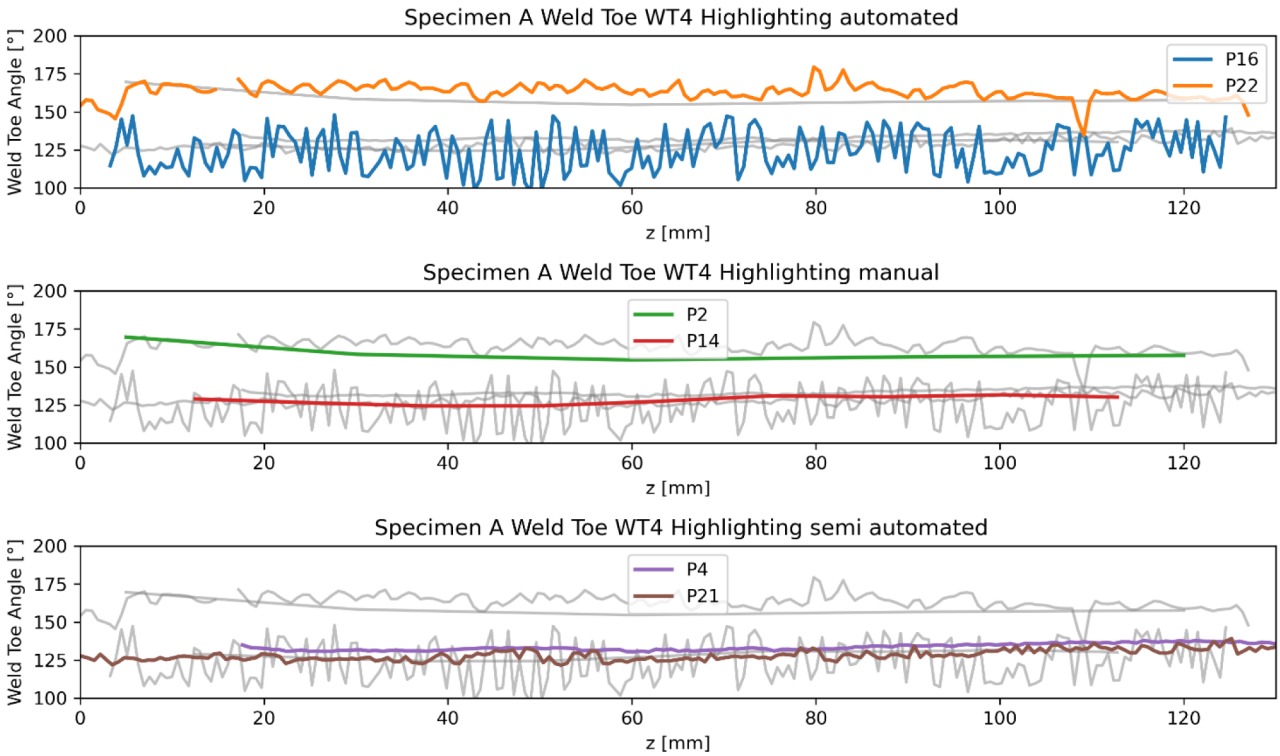

(b) Weld toe angle α of weld toe 4

Fig. 12 Line plot of the weld toe angle for fully-automatic measurements of specimen IIW-A

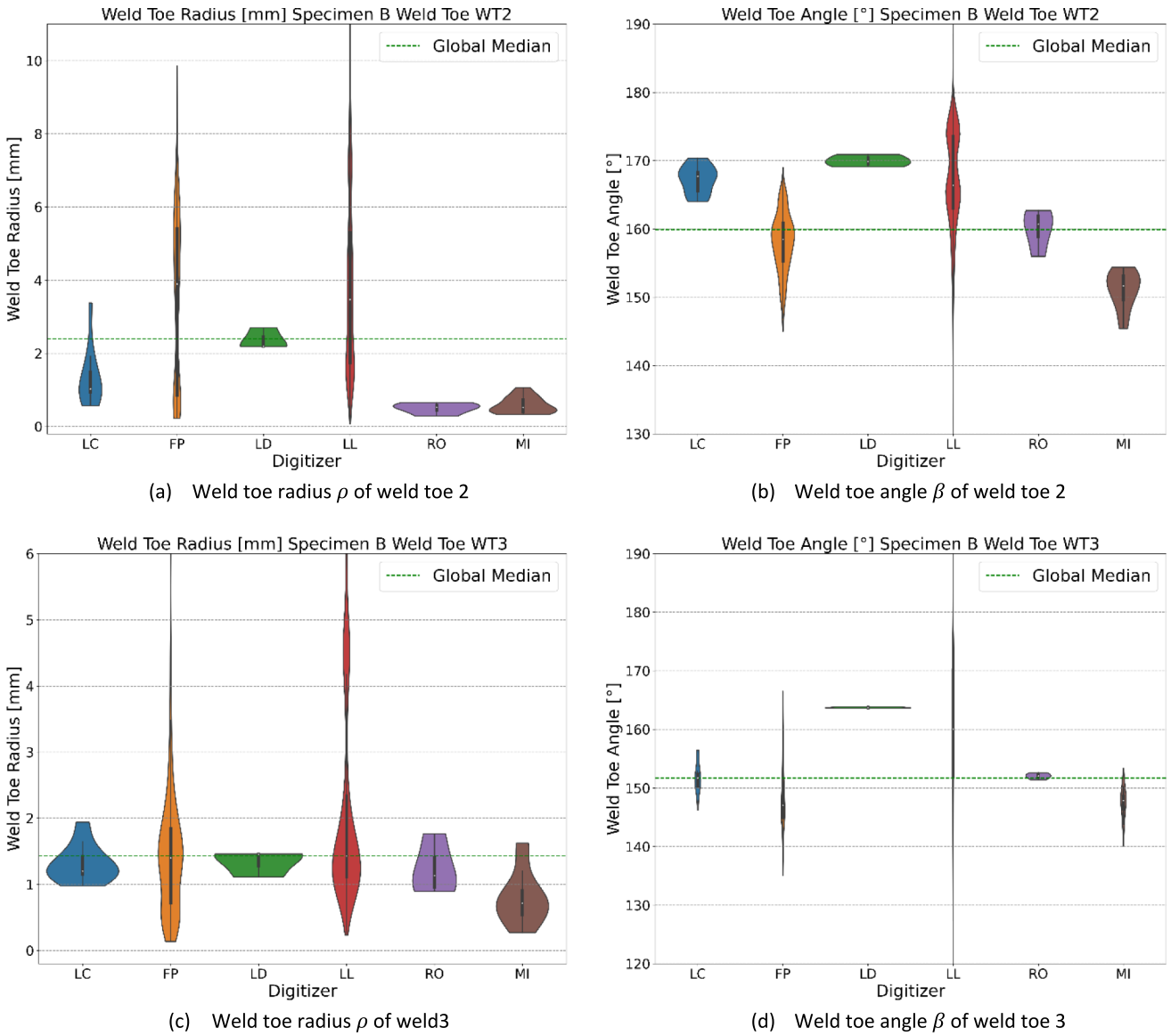

(a) Weld toe radius ρ of weld toe 2

(b) Weld toe angle β of weld toe 2

(c) Weld toe radius ρ of weld3

(d) Weld toe angle β of weld toe 3

Fig. 13 Violin plot of the results for different digitizer for specimen IIW-B

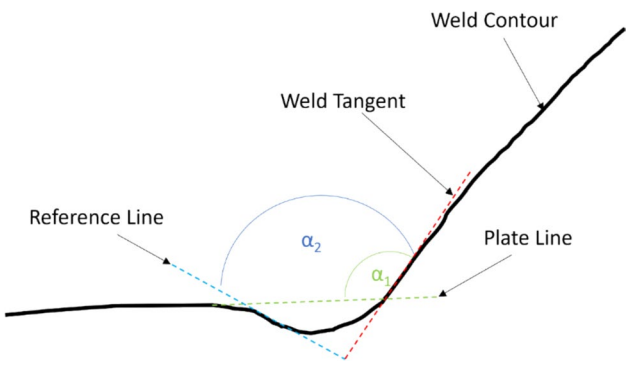

Fig. 14 Possible definitions of the weld toe angle for HFMI treated weld

has a larger radius and a higher scatter. The bottom weld toe is smaller, and the results are closer to each other.

The results of part A and part B show differences. The authors assume that a main challenge is that no uniform definition and clear contour of the weld toe radius is given. While the machined specimens of part A had a clearly defined weld toe, it is not the case for the welded specimens of part B. Another reason can be the different weld geometry along the weld seam. The local weld geometry differs along the weld seam. However, the line plot in Fig. 11b show different peaks along the weld seam. Since the HFMI process generates a uniform weld toe radius, measurement inaccuracy of the individual participants cannot be ruled out.

6 Conclusion

Three different welded specimens are measured by different participants to compare the influence of the measurement methods. The parameters to be measured are the weld toe radius ρ and weld toe angle α. In addition, the influence of the weld geometry, the level of automation, and the digitizers used is considered. The following observations are made:

- The individual data series provided by the participants do not show uniform measurement results for the weld toe radii. This phenomenon is even more pronounced with flat weld seams. The higher the values of weld toe radii are, the greater the deviations between the individual participants. For the HFMI-treated weld (specimen IIW-A weld toe 4), the measurement results for the weld toe radii vary even more than in the as-welded condition.
- For the weld toe angles, the participants also achieve different measurement results. The largest differences occur at the HFMI-treated weld toe (specimen IIW-A weld toe 4). A different approach to defining the weld toe angle for the HFMI-treated weld toe is assumed to be the reason. For the flat weld seams (specimen IIW-A weld toe 2 and weld toe 3), the angle measurements are comparable.
- Manual measurements of the weld toe parameters show the lowest scatter. Larger deviations are more likely to be found with the semi-automated and fully automated methods. However, the participants using manual methods provided significantly fewer measuring points. This may be related to the higher effort required for manual measurements.
- An influence of the digitizer is not evident in this study. It turns out that the evaluation method has a greater influence than the digitizer. However, only laser line sensors and fringe projection sensors can be compared with each other, as there are too few participants for the other types of digitizers.

A major challenge with comparability between the data series of the participants is that a different number of measured values were provided. Compared to part A, there are greater differences between the single results in the current study. Since the weld toe parameters are not a priori known, it is not possible to evaluate the methods according to their accuracy, but only according to their performance compared to the other participants. As the individual evaluation methods are not exactly known and for the majority of participants only the results are available, it cannot be concluded whether the raw data or the evaluation method is responsible for the deviations from one another. The influences of the raw data can be tested by measuring all scan data with only one evaluation method. Thus, the influence of the individual digitizers or the resolution can be clarified. However, this requires additional digitizers in addition to the laser line sensors and fringe projection sensors.

The results demonstrate that a standardized measurement and evaluation method is essential to achieve consistent and comparable results. Given that manual methods, while precise, are labor-intensive and produce only a limited number of measurements, the focus should be on improving automated or semi-automated methods. The goal is to transfer the precision of manual methods to these automated techniques, enabling a higher measurement throughput without compromising accuracy. This would significantly enhance the applicability of weld toe parameter evaluation in industrial and research contexts.

Authors contribution Finn Renken: writing—original draft, visualization, validation, conceptualization, methodology, software, investigation, formal analysis; Jan Schubnell: writing—original draft, conceptualization, supervision; Matthias Jung: writing—review and editing; Moritz Braun: writing—review and editing, conceptualization, supervision; Heikki Remes: conceptualization, supervision.

Funding Open Access funding enabled and organized by Projekt DEAL.

Data availability The anonymized raw data from the participants is available on GitHub.

Declarations

Competing interests The authors declare no competing interests.

References

1. International Organization of Standardization (ISO), (5817:2023) - Welding – Fusionwelded joints in steel, nickel, titanium and their alloys (beam welding excluded) – Quality levels for imperfections

2. Volvo Group (2016) STD 181-0004 Standard Fusion Welding, Issue 4, Page 1–20
3. Hobbacher AF, Baumgärtner J (2024) Recommendations for fatigue design of welded joints and components. 3th illust. Springer
4. Schork B et al (2017) The effect of the local and global weld geometry as well as material defects on crack initiation and fatigue strength. Eng Fract Mech 198:103–122. https://doi.org/10.1016/j.engfracmech.2017.07.001
5. Schork B, Zerbst U, Kiyak Y, Kaffenberger M, Madia M, Oechsner M (2020) Effect of the parameters of weld toe geometry on the FAT class as obtained by means of fracture mechanics-based simulations. Weld World 64(6):925–936. https://doi.org/10.1007/S40194-020-00874-7/FIGURES/14
6. Ning Nguyen T, Wahab MA (1995) A theroretical study of the effect of geometry parameters on the fatigue crack propogation life. Eng Facture Mech 51(1):1–18
7. Lieurade HP, Huther I, Lefebvre F (2008) Effect of weld quality and postweld improvement techniques on the fatigue resistance of extra high strength steels. Weld World 52(7–8):106–115
8. Barsoum Z, Jonsson B (Apr.2011) Influence of weld quality on the fatigue strength in seam welds. Eng Fail Anal 18(3):971–979. https://doi.org/10.1016/J.ENGFAILANAL.2010.12.001
9. Barsoum Z, Samuelsson J, Jonsson B, Björkblad A (2012) Fatigue design of lightweight welded vehicle structures: influence of material and production procedures. Proc Inst Mech Eng Part B J Eng Manuf 226(10):1736–1744. https://doi.org/10.1177/0954405412458046
10. Schubnell J et al (2024) Approach for the probabilistic fatigue assessment of welded joints based on the local geometry of the weld seam. Fatigue Fract Eng Mater Struct 47(1):88–107. https://doi.org/10.1111/FFE.14170
11. Lassen T (1990) The effect of the welding process on the fatigue crack growth. Weld J pp 75–82
12. Renken F et al (Aug.2021) An algorithm for statistical evaluation of weld toe geometries using laser triangulation. Int J Fatigue 149:106293. https://doi.org/10.1016/J.IJFATIGUE.2021.106293
13. Hultgren G, Myrén L, Barsoum Z, Mansour R (2021) Digital scanning of welds and influence of sampling resolution on the predicted fatigue performance: modelling, experiment and simulation. Met 11(5):822. https://doi.org/10.3390/MET11050822
14. Schubnell J et al (Feb.2020) Influence of the optical measurement technique and evaluation approach on the determination of local weld geometry parameters for different weld types. Weld World 64(2):301–316. https://doi.org/10.1007/s40194-019-00830-0
15. Jung M, Braun M, Schubnell J, Remes H (2024) Round robin study on the determination of weld geometry parameters - part A: analysis of a reference specimen. Weld World. https://doi.org/10.1007/s40194-024-01829-y
16. Schubnell J, Ladendorf P, Sarmast A, Farajian M, Knödel P (2021) Fatigue performance of high-and low-strength repaired welded steel joints. Met (Basel) 11(2). https://doi.org/10.3390/met11020293
17. Braun M, Ahola A, Milaković AS, Ehlers S (Feb.2022) Comparison of local fatigue assessment methods for high-quality butt-welded joints made of high-strength steel. Forces Mech 6:100056. https://doi.org/10.1016/J.FINMEC.2021.100056
18. Braun M, Scheffer R, Fricke W, Ehlers S (Feb.2020) Fatigue strength of fillet-welded joints at subzero temperatures. Fatigue Fract Eng Mater Struct 43(2):403–416. https://doi.org/10.1111/FFE.13163